Available online at www.sciencedirect.com
ScienceDirect
International Journal of Heat and Mass Transfer 50 (2007) 4780–4795
International Journal of HEAT and MASS TRANSFER
www.elsevier.com/locate/ijhmt

1D plane numerical model for boiling liquid expanding vapor explosion (BLEVE)

G.A. Pinhasi [a,*], A. Ullmann [b], A. Dayan [b]

[a] Department of Chemical Engineering and Biotechnology, Faculty of Engineering, The College of Judea and Samaria, Ariel, Israel
[b] Department of Fluid Mechanics and Heat Transfer, Faculty of Engineering, Tel-Aviv University, Tel-Aviv, Israel

Received 24 May 2006; received in revised form 14 February 2007
Available online 25 May 2007

Abstract

The depressurization of a vessel containing saturated or subcooled liquid may occur in a variety of industrial processes and often poses a potentially hazardous situation. A 1D plane numerical model was developed for estimating the thermodynamic and the dynamic state of the boiling liquid during a boiling liquid expanding vapor explosion (BLEVE) event. Based on the choice of the initial nucleation sites density, the model predicts, simultaneously, the bubble growth processes in the liquid at the superheat-limit state, the front velocity of the expanding liquid, and the shock wave pressure formed by the liquid expansion through the air.

Conditions of shock formation were found to be normally associated with high initial temperatures that can bring the liquid to its superheat-limit state during the initial depressurization. Furthermore, the high initial temperature also induces a generation of higher vapor pressures that forces a rapid mixture expansion.

Model predictions of the shock wave strengths, in terms of TNT equivalence, were compared against those obtained by simple energy models. As expected, the simple energy models over predicts the shock wave strength. However, the simple model which accounts for the expansion irreversibility, produces results which are closer to current model predictions.

Keywords: BLEVE; Blast pressure; Explosions; PLG; Flashing; Safety

1. Introduction

Storage tank failure accidents may result from a sudden rupture of a pressure vessel containing saturated or subcooled liquid that initiates a blowdown transient release. The most severe form of release is the boiling expanding vapor explosion (BLEVE). It is usually associated with a large explosive release of Pressure Liquefied Gasses (PLG's). The explosive part of the release is caused by a very rapid phase change from liquid to vapor, and is characterized by shock wave formations. A comprehensive review on the exploration of the phenomenon could be found in Leslie and Birk [1], and the case history in Lees [2] (vol. 3).

Historically, the majority of the BLEVE accidents are associated with a storage of flammable liquids such as propane and butane. Surrounding fire caused ignition, which then propagated to a fireball. In a broad definition of a BLEVE, as used by Klets [3] and Lees [2], it is assumed that any liquefied vapor – flammable or non-flammable – can cause a BLEVE.

Prugh [4] has reviewed the events that precede a BLEVE accident. In the standard scenario, a tank of liquefied gas, usually propane is engulfed in a fire. As the fire heats the tank, the temperature and pressure of its fluid rise, roughly through a saturation path (excluding temperature stratification effects). The metallic vessel losses its strength and eventually raptures, exposing its fluid to atmospheric pressure. Being at a temperature well above its boiling

* Corresponding author.
E-mail addresses: gadip@yosh.ac.il (G.A. Pinhasi), ullmann@eng.tau.ac.il (A. Ullmann), dayan@eng.tau.ac.il (A. Dayan).

0017-9310/$ - see front matter © 2007 Elsevier Ltd. All rights reserved.
doi:10.1016/j.ijheatmasstransfer.2007.03.016

Nomenclature

A	cross-section area
$\tilde{A}_i$	interfacial area density
a	speed of sound
C	constant
C_P	specific heat constant pressure
C_V	specific heat constant volume
$C^{\pm}$	characteristic path
$\mathrm{D}/\mathrm{D}t$	material derivative
$\mathrm{D}^{\pm}/\mathrm{D}t$	wave derivative
E	internal energy
e	specific internal energy of phase k
f	force per unit volume
g	gravitational acceleration
h	convection heat transfer coefficient
h_k	specific enthalpy of phase k
h_{LG}	latent heat of evaporation
Ja	Jakob number
k_{B}	Boltzmann's constant
k_k	thermal conductivity of phase k
L_0	initial liquid length
m	Mass
m_{T}	overall mass in the vessel
m_{TNT}	mass of explosive (TNT)
m_{M}	mass of a molecule
M	Mach number
n_{B}	bubble number-density
n_{d}	droplet number-density
Nu	Nusselt number
P	pressure
$P_{\min}$	static pressure at the flashing inception point
PP	particle path
q	heat transfer rate
$q''_{\mathrm{i,net}}$	heat diffusion rate from the liquid to the bubble
r	distance
R_{B}	bubble radius
R_{d}	droplet radius
RW	rarefaction wave
s	entropy
T	temperature
t	time
u	velocity
v	velocity relative to the shock wave
V	volume
W	work
W_{flash}	expansion work
x	coordinate
Z	elevation
z_{SD}	scaled distance

Greek symbols

α	volumetric void fraction
χ_{flash}	quality at the end of flashing process
δ	parameter
$\Delta P_{\mathrm{under}}$	pressure undershoot
$\Delta P_{\mathrm{shock}}$	shock overpressure
ε_k	void fraction of phase k
$\Gamma_{i,k}$	mass transfer rate of phase k
γ	specific-heat ratio
ρ	density
σ	surface tension
υ	specific volume
Π	dimensionless shock strength

Subscripts

air	air
atm	atmospheric conditions
B	bubble
c	thermodynamic critical conditions
G	gas phase
i	interfacial
k	phase index (G = gas, L = liquid)
L	liquid phase
m	mixture
min	flashing inception point
SL	superheat-limit
sat	saturation
Shock	shock
sup	superheat
w	wall
0	initial value
∞	infinity
1	side where the fluid enters the shock wave
2	side where the fluid leaves the shock wave

Superscript

$''$	area flux

point, the superheated fluid boils rapidly and often violently.

Few large and small-scale experiments were conducted to study the BLEVE phenomenon. McDavitt et al. [5] recorded the pressure response in a shock tube to study the BLEVE initiation. Melhem et al. [6] performed BLEVE experiments using a propane tanks. Venart et al. [7] reported the possibility of another type of failure that is more powerful than the BLEVE. The event is a boiling liquid compressed bubble explosion (BLCBE). Stawczyk [8] described experiments with explosions of small LPG tanks.

Theories explaining the BLEVE are few in number and rely on scarce data [1]. Reid [9] suggested that BLEVE's are essentially superheat explosions, and therefore can be predicted by superheat-limit considerations. The expansion of a sufficiently superheated liquid is accompanied by a high rate of microscopic vapor bubble formation. The extent of superheat necessary for sustaining high rates of bubble

formation can be determined from the homogeneous nucleation theory, or alternatively by the superheat-limit temperature, T_{SL}. For a wide range of substances the ratio between the superheat temperature at ambient pressure, $T_{SL}(P_{atm})$, and the critical temperature, $T_{SL}(P_{atm})/T_c$, lies within the range 0.89–0.90.

BLEVE scenarios can be described by the super-heat limit theory for certain conditions of liquefied gas vessels depressurization [9]. Initially, prior to failure, the vessel containing both vapor and liquid is at a saturated state. Following the vessel failure, the depressurization process takes place. Two possible depressurization processes from the saturation line are illustrated in Fig. 1. If the depressurization occurs at a relatively low temperature, corresponding to point A, the pressure falls to the atmospheric pressure B. Such depressurization may exhibit violent boiling features. However, vapor explosion would not occur since the superheat-limit (seen as a doted line) cannot be reached. If depressurization occurs from a higher temperature, point C, the pressure would fall to point D. Here the superheat-limit line is reached and a vapor explosion occurs. In essence, it means that the liquid reaches the superheat-limit prior to phase transition [10]. The superheat-limit temperature at atmospheric pressure is thus a temperature threshold below which a superheated liquid explosion cannot occur.

In support of this hypothesis Reid quotes experiments by Anderson and Armstrong [11], as well as a number of industrial accidents, as being consistent with the hypothesis. His explanation is generally regarded as one of merit. Subsequent work efforts by, Martinsen et al. [12], McDevitt et al. [13], Davenport [14], Dunn [15] and Venart et al. [7] also support the superheat-limit explanation. BLEVE's are usually form shock waves. However, there are no fully validated models to predict those shock waves.

Yu and Venart [16] presented a preliminary physical and mathematical model to describe the behavior of the BLCBE. The simple numerical model computes the propagation of, both, depressurization and compression waves caused by mass discharge through cracks, and also calculates the rise of the liquid–vapor interface owing to void generation.

Van den Berg et al. [17,18] presented a method to calculate the blast effects originating from an exploding vessel of liquefied gas. The blast overpressure from a BLEVE was numerically computed by imposing the vapor pressure of a flashing liquid as boundary condition for the gas dynamics code. This was done without any modeling of the flashing process. Additionally, it was demonstrated that often, reasonable estimates of BLEVE blast effects could be obtained from simple expansion of acoustic volume source considerations.

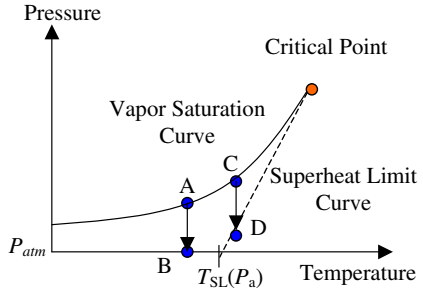

Fig. 1. Reid's theory for BLEVE formation on schematic figure of vapor saturation and superheat curves [9].

Deligiannis and Cleaver [19] presented a two-phase model for the blowdown of a partially full vessel. They used a simple model, consisting of the centered expansion fan equations, to predict the average vapor pressure and velocity of the vessel outflow.

The initial shock wave pressure and the blast effect are usually evaluated in terms of energy parameters and expressed as TNT equivalents [4,20]. The energy calculations are frequently based on the assumption of reversible adiabatic expansion during the decompression from the initial pressure to atmospheric pressure [4]. Planas-Cuchi et al. [20] calculated the energy, based on a more realistic assumption of irreversible adiabatic expansion.

The purpose of the current work was to develop a model for estimating the thermodynamic and the dynamic state of the boiling liquid during the BLEVE event. Based on the choice of the initial nucleation sites density, the model predicts the bubble growth in the liquid at the superheat-limit state. It addresses the front velocity of the expanding liquid and the shock wave pressure formed by the liquid expansion through the air. A novel model is given which describes the coupling of two-phase flashing flow with compressible airflow. Model predictions were compared to the results of the two TNT models. Such a 1D plane shock formation and propagation can be associated with a BLEVE scenario in a tunnel, or within any other type of cylindrical conduit.

2. The model

The BLEVE model is based on coupling two models for one-dimensional plane unsteady flow: a model of expanding two-phase mixture with compressible ideal gas (air) flow model with or without shock waves. A convenient description of the motion of air during a BLEVE is through the "1D plane Piston Problem" simulation. The piston is a representation of the front boundary of an expanding two-phase mixture.

2.1. Model formulation

Consider a one-dimensional flow of air that is driven by a rapid boiling expansion of a two-phase boiling mixture behind it. The boiling is a consequence of the sudden exposure of compressed high temperature liquid to atmospheric pressure.

The BLEVE scenarios are initialized by a propagation of a depressurization wave away from the break location into the high-pressure liquid. The depressurization wave, rarefaction wave, RW, propagates into the liquid at the

liquid speed of sound. During its propagation, the compressed fluid is depressurized to a level well below the saturated pressure of the initial temperature (pressure-undershoot). The penetration of a superheated fluid into a metastable thermodynamic state triggers an extremely fast process of vapor nucleation. The rapidity of the bubble nucleation and growth processes is of substantial influence on the blowdown and BLEVE scenarios [21].

The vigor vapor generation is the cause for the rapid surge of the two-phase mixture volume. The acceleration of the interface between the two-phase mixture and the air is the reason for the compression of the air front. As a result of the rapid acceleration, the contact surface velocity may reach the speed of sound in the air, thereby forcing the development of a shock wave. The rate of acceleration and the formation of the shock wave depend primarily on the liquid initial thermodynamic state.

A schematic diagram of the process is shown in Fig. 2. The initial state is depicted at the bottom of the figure. The vessel wall separates the compressed liquid from the ambient air. At time $t = 0$ the liquid is suddenly exposed to the low ambient pressure and the rarefaction wave expands into the liquid (to the left side). Whereas, both, the mixture–air contact interface and the shock wave propagate to the right. The figure reveals schematically the expansion of all waves by there $x = f(t)$ dependence. The four regions characterizing the depressurization process are indicated at near the top of the figure. Sequentially, the regions are: compressed liquid, liquid–vapor mixture, compressed air and undisturbed ambient air. The pressure profile for the indicated intermediate expansion stage is presented at the figure top.

The current model consists of two parts, one for the two-phase mixture and the other for the air. The coupling between the two regions takes place at the interface. The latter is actually a common moving boundary for each of the two domains. The possible presence of a shock wave is accounted for in the model as a discontinuity within the air domain. Viscous effects, such as in between phases or at boundaries, are assumed to be negligible.

2.2. Two-phase model

The present two-phase flow analyses are based on the equal velocities unequal temperatures (EVUT) model, for which the existence of equal local pressure between phases (i.e. $P_L = P_G = P$), no slip conditions (i.e. $u_L = u_G = u$) and no interfacial friction, ($f_{i,k} = 0$) are assumed. According to these assumptions, the one-dimensional conservation equations (continuity, momentum and energy) reduce to:

$$\frac{\partial}{\partial t}[\varepsilon_k \rho_k] + \frac{\partial}{\partial x}[\varepsilon_k \rho_k u] = \Gamma_{i,k} - \varepsilon_k \rho_k u \frac{1}{A}\frac{\mathrm{d}A}{\mathrm{d}x} \tag{1}$$

$$\rho \frac{\partial u}{\partial t} + \rho u \frac{\partial u}{\partial x} + \frac{\partial P}{\partial x} = -(f_{w,L} + f_{w,G}) - \rho g \frac{\mathrm{d}Z}{\mathrm{d}x} \tag{2}$$

$$\varepsilon_k \rho_k \frac{\partial h_k}{\partial t} + \varepsilon_k \rho_k u \frac{\partial h_k}{\partial x} + \varepsilon_k \frac{\partial P}{\partial t} - \varepsilon_k u \frac{\partial P}{\partial x} = q_{i,k} + q_{w,k} + f_{w,k} u \tag{3}$$

In these equations, the subscript k(L or G) denotes the phase (liquid or vapor, respectively). The flow and liquid properties ε_k, ρ_k, u_k, P_k and h_k are the volume fraction, density, axial velocity, pressure and the specific enthalpy of phase k, respectively. The source terms $\Gamma_{i,k}$, $f_{w,k}$, $q_{i,k}$ and $q_{w,k}$ are the mass transfer rate at the interface, wall friction, interfacial heat transfer and wall heat transfer into phase k per unit volume, respectively. Likewise, A is the cross-section area of the duct, Z the elevation, g the gravitational acceleration, and t and x are the time and the space independent variables. The mixture density is given by $\rho = \varepsilon_G \rho_G + \varepsilon_L \rho_L$ and the void fraction is $\alpha \equiv \varepsilon_G$.

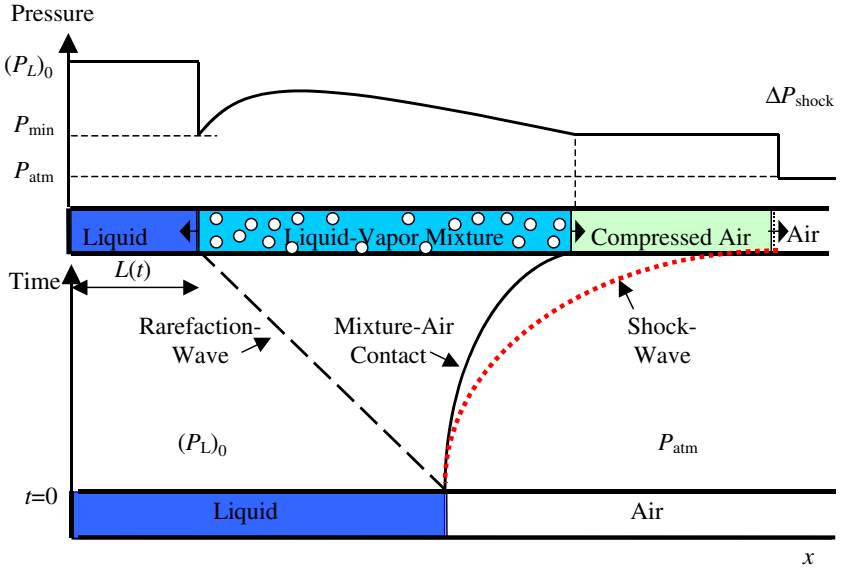

Fig. 2. Typical wave action in the $x - t$ plane and the pressure profile following BLEVE.

The set of equations is subject to the thermodynamic state equation of each phase:

$$\rho_k = \rho_k(P, h_k) \tag{4}$$

2.2.1. The constitutive equations

The constitutive equations for wall and interfacial heat and mass transfer must be provided for closure. A simple flow regime maps [22] is adopted which consists of bubbly flow for void fractions less than 0.3, droplets flow for void fractions larger than 0.7, and transition regime (churn turbulent flow) for void fractions between 0.3 and 0.7. As customary in the modeling of two-phase flashing flows and for simplicity, it is assumed that the bubble growth is fully thermally controlled (free of the initial inertia controlled stage).

The rate of vapor generation is limited by the heat transfer rate and interfacial area as:

$$\Gamma_{i,G} h_{LG} = q_{i,net} \tag{5}$$

where $h_{LG} = h_G - h_L$ is the latent heat and $q_{i,net} = q_{iL} - q_{iG}$ is the heat input from the liquid to the bubble–liquid interface. The net interfacial heat flux, $q''_{i,net}$ and the net mass flux $\dot{m}''_i$ are defined as

$$q_{i,net} = \tilde{A}_i q''_{i,net} \quad \Gamma_{i,G} = \tilde{A}_i \dot{m}''_i \tag{6}$$

where $\tilde{A}_i$ is the interfacial area density (area per unit volume). The interfacial area density has to be determined according to the two-phase flow regime. The source terms of the governing equations, the evaporation rates and friction force terms, are all described by Pinhasi [23].

2.2.2. Bubbly flow regime

For bubbly flow, $\alpha < 0.3$, it is assumed that all of bubble nucleation sites are formed within a very short time during the sharp depressurization. The growth of those bubbles proceeds at a slower pace. Therefore it can be assumed that the bubbles, having similar diameters, can be characterized by an average size for any given cross-section (but varies from one cross-section to another). For spherical bubbles, the interfacial area density $\tilde{A}_i$ is given by

$$\tilde{A}_i = 4\pi R_B^2 n_B \tag{7}$$

where n_B is the bubble number density and R_B is the bubble radius. Also

$$\alpha = \frac{4}{3}\pi R_B^3 n_B = \frac{1}{3}\tilde{A}_i R_B \tag{8}$$

so that

$$\tilde{A}_i = \frac{3\alpha}{R_B} = (36\pi n_B)^{1/3}\alpha^{2/3} \tag{9}$$

The bubble growth is assumed to be heat diffusion controlled. Therefore the heat supply to the bubble interface can be expressed as

$$q''_{i,net} = h\Delta T_{sup} \tag{10}$$

where ΔT_{sup} is the liquid superheat, $\Delta T_{sup} = T_L - T_{sat}(P)$ (the subscript "sat" indicates saturation).

The heat transfer coefficient, h, is taken from solutions for the diffusion rate of heat transport from a liquid at a constant superheat state to a bubble interface, which is

$$h = \frac{k_L Nu}{2R_B} \tag{11}$$

The Nusselt number in this expression is a function of the Jakob number, according to, [24]:

$$Nu = \frac{12}{\pi} Ja \left[1 + \frac{1}{2}\left(\frac{\pi}{6Ja}\right)^{2/3} + \frac{\pi}{6Ja}\right] \tag{12}$$

where the Jakob number is defined as

$$Ja \equiv \frac{C_{P,L}\rho_L \Delta T_{sup}}{\rho_G h_{LG}} \tag{13}$$

In this case, $C_{P,L}$ is the specific heat of the liquid, and h_{LG} is the latent heat. Eq. (12), in general is valid only for a uniform superheat and not for variable pressure fields [25]. However, it has been shown to be quite accurate for non-uniform conditions, provided that local superheat values are used [26].

For extensive superheat conditions, near the superheat-limit (spinoidal), the rate of evaporation and condensation of molecules at the vapor–liquid interface is governed by statistical mechanics laws of transport and according to [10] is

$$\dot{m}''_i = \frac{1}{\sqrt{2\pi m_M 1 k_B T}}(P_{sat} - P_G) \tag{14}$$

where k_B is the Boltzmann's constant, and m_M is the mass of a molecule.

2.2.3. Churn-turbulent flow regime

For bubbly-droplets transition regime flow, $0.3 < \alpha < 0.7$, it is assumed that some of the bubbles coalesce and form larger (Taylor) bubbles. If the void fraction exceeds 0.3, two opposing effects influence the surface area density. On one hand, the continuing bubble growth, distortion of their shape and bubble breakup tends to increase the area density, $\tilde{A}_i$. On the other hand, the coalescence and formation of large bubbles tends to reduce $\tilde{A}_i$. The variation of $\tilde{A}_i$ with void fraction is small. It is therefore assumed that $\tilde{A}_i$ has a constant value corresponding to $\alpha = 0.3$, which represents a geometric condition above which bubble coalescence must take place. The heat flux and the heat transfer coefficient for bubbly-droplets transition flow regime were taken as for bubbly flow with $\alpha = 0.3$ using Eqs. (10) and (11).

2.2.4. Droplets flow regime

For the case of transitional and dispersed droplet flows $\alpha > 0.7$, the heat and mass transfer occur on the liquid droplets. The droplets are formed as a result of bubble coagulation and droplet entrainment from the lateral

surface of large Taylor bubbles. The interfacial area density for those conditions is given by

$$\tilde{A}_{\mathrm{i}} = \frac{3(1-\alpha)}{R_{\mathrm{d}}} \tag{15}$$

where R_{d} is the droplet diameter. For this case, the net interfacial heat flux is

$$q''_{\mathrm{i,net}} = \frac{k_{\mathrm{L}} Nu}{2R_{\mathrm{d}}}(T_{\mathrm{L}} - T_{\mathrm{G}}) \tag{16}$$

The Nusselt number is assumed to be constant at a value of $Nu = 16$, as suggested by Solbring et al. [27]. The transition to dispersed droplet flow, as previously mentioned, occurs at $\alpha > 0.7$ and has an interfacial area density of

$$\tilde{A}_{\mathrm{i}} = \frac{3(1-\alpha)}{R_{\mathrm{d}}} = (36\pi n_{\mathrm{d}})^{1/3}(1-\alpha)^{2/3} \tag{17}$$

The variation with α, for simplicity is assumed to be symmetrical around $\alpha = 0.5$. Thus $\tilde{A}_{\mathrm{i}} \sim \alpha^{2/3}$ if $\alpha < 0.3$ (Eq. (9)), and $\tilde{A}_{\mathrm{i}} \sim (1-\alpha)^{2/3}$ if $\alpha > 0.7$.

2.3. Air model

The governing conservation equations for one-dimensional unsteady compressible flow of gas are presented [28,29]. The flow is considered as confined within a duct of known cross-sectional area, $A(x)$. The continuity and momentum equations for the flow are

$$\begin{aligned} &\frac{\partial \rho}{\partial t} + \frac{1}{A}\frac{\partial (A\rho_{\mathrm{air}} u_{\mathrm{air}})}{\partial x} = 0 \\ &\frac{\partial}{\partial t}(\rho_{\mathrm{air}} u_{\mathrm{air}}) + \frac{1}{A}\frac{\partial}{\partial x}(A\rho_{\mathrm{air}} u_{\mathrm{air}}^2) + \frac{\partial P_{\mathrm{air}}}{\partial x} = -f_{\mathrm{w,air}} \end{aligned} \tag{18}$$

where ρ_{air} is the air density, u_{air} is the air velocity, P_{air} is the air pressure, whereas x and t are the independent variables that denote the distance and the time, respectably. The equation for isentropic conditions is

$$\frac{\partial s_{\mathrm{air}}}{\partial t} + u_{\mathrm{air}}\frac{\partial s_{\mathrm{air}}}{\partial x} = 0 \tag{19}$$

where s_{air} is the entropy of the air. The isentropic assumption states that there are no entropy changes for fluid particle.

In the present model, the flow is considered as isentropic. This assumption is not as restrictive as the assumption of a homentropic flow. For isentropic flow, the entropy of each fluid particle does not change with time, Eq. (19), but the entropy of different fluid particles may be different, $\nabla s \neq 0$. Physically, this situation could be present in a fluid that was initially with non-uniform entropy, or a fluid that non-uniform entropy was caused by the passage of a changing shock wave (variable strength with time). This is in contrast with the homentropic assumption that states that there are no entropy gradients in front and behind the shock wave, i.e. $\mathrm{D}s/\mathrm{D}t = \nabla s = 0$ within each domain.

The isentropic assumption implies that viscous dissipation and heat transfer effects are negligible. It is important to note that no such assumption is made for the narrow region occupied by the shock wave. There, explicitly, the specific entropy undergoes a finite jump. Therefore analyses of the shock wave region are conducted separately.

2.3.1. The shock wave

A shock wave is confined within a relatively thin region. A normal shock wave separates two regions, one of sonic velocity and the other of subsonic. The shock wave region is referred to as a surface of discontinuity, across which most of the fluid properties change. The model calculates the conditions across the moving shock using the shock relations.

It is convenient to conduct shock wave analyses with a set of stationary coordinates relative to the shock wave. The transformation of a moving shock wave into a stationary frame of reference is conducted according to $v_1 \equiv u_{\mathrm{shock}} - u_1$ and $v_2 \equiv u_{\mathrm{shock}} - u_2$, where u is denotes absolute fluid velocities, v is the fluid velocities relative to the shock (directed to $-x$ direction) and u_{shock} the shock-wave velocity. Side 1 is referred to the side where the fluid enters a control volume (here the shock wave) and side 2 is the side where the fluid leaves the control volume.

The shock Mach number defined as

$$M_{1n} = \frac{v_1}{a_1} \tag{20}$$

where a is the air speed of sound. The flow properties, pressure, velocity, density and Mach number behind the shock wave ($P_2, v_2, \rho_2 = 1/v_2, M_{2n} = v_2/a_2$) are represented in the model in terms of the shock Mach number, M_{1n} [28].

The shock properties that are presented are the shock over-pressure and dimensionless shock strength, Π, defined as

$$\Pi = \frac{P_2 - P_1}{\rho_1 a_1^2} \tag{21}$$

where $P_2 - P_1$ is the shock pressure, ρ_1 and a_1 are the density and the speed of sound of the air low-pressure side of the shock, respectively.

2.4. Coordinate systems

The model can be applied to 1D plane, cylindrical or spherical flow. Expanding the continuity and momentum equations for both regions and noting that the cross-sectional area A depends only on space coordinate x, the area derivative can be written as

$$\frac{1}{A}\frac{\mathrm{d}A}{\mathrm{d}x} = \frac{\delta}{x} \tag{22}$$

where δ is parameter for the coordinate system: For 1D plane case $\delta = 0$, or for the cylindrical flow in which the space coordinate is the distance from the axis and the velocity is directed away from (or toward) the axis $\delta = 1$, and for spherical flow in which the space coordinate is the distance from one point, chosen as the origin, and the velocity is directed away from (or toward) this point $\delta = 2$.

2.5. Initial and boundary conditions

The initial conditions of interest in the present study are those of either subcooled or saturated liquids with a uniform pressure (P_0) and temperature (T_0). The ambient air is initially at rest ($u_{air} = 0$) with standard atmospheric pressure and temperature, $P_{air,0}$; $T_{air,0}$.

The boundary conditions are as followed. At the left end, ($x = 0$), the fluid is stationary ($u = 0$); At the mixture/air interface, $x = L(t)$, continuity of pressure and velocity exist across the interface, i.e. $P_m = P_{air}$, and $u_m = u_{air}$; and at far right hand side end, $x = \infty$, the air is stationary and undisturbed, i.e. $u_{air} = 0$ and $P_{air} = P_{atm}$.

$t < 0$	$0 \leqslant x \leqslant L_0$	Liquid	$P_m = P_0;\ T_m = T_0;\ \alpha = 0;\ u_m = 0$
	$x > L_0$	Air	$P_{air} = P_{air,0};\ T_{air} = T_{air,0};\ u_{air} = 0$
$t = 0$	$x = L_0$	Contact	$P_m = P_{air};\ u_m = u_{air} = 0$
$t > 0$	$x = 0$	Liquid	$\frac{\partial P_m}{\partial t} = \frac{\partial T_m}{\partial t} = 0;\ u_m = 0$
	$x = L_0 - a_L t$	RW	$P_m = P_{min};\ u_m = 0;\ n_B = n_{B,0};\ R_B = R_{B,0};$
	$x = L(t)$	Contact	$P_m = P_{air};\ u_m = u_{air}$
	$x \to \infty$	Air	$P_{air} = P_{air,0};\ T_{air} = T_{air,0};\ u_m = 0$

(23)

At time zero, the liquid at one end ($x = L_0$), is exposed to the ambient atmospheric pressure, where L_0 is the initial liquid length. As a result, a rarefaction wave, RW, propagates into the liquid at the liquid speed of sound, a_L. In the depressurization process the fluid drops to a minimum pressure P_{min}. This minimum can be, either, the pressure-undershoot ($\Delta P_{under} = P_{sat}(T_0) - P_{min}$), calculated according to the flashing inception model of Elias and Chambre [30] for the case of $T_0 < T_{ST}(P_0)$, or the spinoidal-line intersect corresponding to the superheat-limit, for $T_0 > T_{ST}(P_0)$ (Fig. 1).

The expansion of a saturated liquid is characterized by the formation of a bubbly two-phase mixture. At relatively low initial temperatures, the value of the initial bubble number-density was chosen so as to support the pressure-undershoot predicted by the pressure-undershoot model of Elias and Chambre [30] (see [31]). The initial number density of the bubble nucleation sites, $n_{B,0}$ is a function of the initial temperature and is taken from published recommended values: 10^8–10^{12} m^{-3} as a function of P_{min} [30].

On the other hand, at higher initial temperatures, conditions should produce a pressure-undershoot that gets to the superheat-limit. Thus the chosen initial bubble number-density was the maximum one, $n_{B,0} = 10^{12}$ [10]. For conditions that leads to the superheat limit, $n_{B,0} = 10^{12}$ m^{-3}.

The initial bubble radius was taken as the bubble critical size at the minimum pressure state ($R_{B,0} = \sigma/(P_{sat}(T_0) - P_{min})$, where σ is the liquid surface tension.

3. The numerical solution

The equations of motion of a rapidly expanding two-phase flow are non-linear and hyperbolic. They also exhibit wave propagation features. Therefore, a numerical scheme that incorporates the method of characteristics to solve the governing equations was developed.

3.1. Characteristic form of equations of motion

After applying the method characteristics analysis to the conservation equations of fluid motion, one can get two types of characteristic directions: a set of characteristic curves $dx/dt = u \pm a$, that is called "waves", and a set of characteristic curves $dx/dt = u$ that is called "streamlines". The derivative-operators correspond to these characteristic curves are the standard material derivative D/Dt and the wave derivative $D^{\pm}/Dt$:

$$\frac{D}{Dt} \equiv \frac{\partial}{\partial t} + u\frac{\partial}{\partial x} \qquad \frac{D^{\pm}}{Dt} \equiv \frac{\partial}{\partial t} + (u \pm a)\frac{\partial}{\partial x} \tag{24}$$

where a is the speed of propagation of a small disturbance in the fluid, i.e., the speed of sound.

$$a^2 = \left(\frac{\partial P}{\partial \rho}\right)_s \tag{25}$$

The derivative operators D^+/Dt and D^-/Dt represent the time rate of change for observer traveling at velocities $u \pm a$, that is, with a positive C^+ or negative C^- sound wave. The curves of the waves C^+, C^- and particle-path PP, appear as lines on the $x - t$ diagram, and known as characteristics lines or simply characteristics.

3.2. Characteristic form of the EVUT equations

The characteristic form of the EVUT equations is obtained from a linear combination of the governing equations (1)–(3) and the equation of state (4), as [32]:

$$\begin{aligned}
&\frac{D^+P}{Dt} + \rho a\frac{D^+u}{Dt} = \rho a^2 C_1 + aC_2\\
&\frac{D^-P}{Dt} - \rho a\frac{D^-u}{Dt} = \rho a^2 C_1 - aC_2\\
&\frac{D^+\alpha}{Dt} - \alpha(1-\alpha)\left(\frac{1}{\rho_L a_L^2} - \frac{1}{\rho_G a_G^2}\right)\frac{D^+P}{Dt} = C_3\\
&\frac{Dh_G}{Dt} - \frac{1}{\rho_G}\frac{DP}{Dt} = C_4\\
&\frac{Dh_L}{Dt} - \frac{1}{\rho_L}\frac{DP}{Dt} = C_5
\end{aligned} \tag{26}$$

The mixture speed of sound that was found by using the characteristics analysis, is

$$a^{-2} = \rho\left[\frac{\alpha}{\rho_G a_G^2} + \frac{1-\alpha}{\rho_L a_L^2}\right] \tag{27}$$

where the speed of sound of each phase is

$$a_k^{-2} = \frac{\partial \rho_k}{\partial P} + \frac{1}{\rho_k}\frac{\partial \rho_k}{\partial h_k} \tag{28}$$

The C_i are given by

$$C_1 = \left(\frac{1}{\rho_G} - \frac{1}{\rho_L}\right)\Gamma_{i,G} - u\frac{1}{A}\frac{dA}{dx} - \frac{\alpha}{\rho_G}\frac{\partial \rho_G}{\partial h_G}C_4 - \frac{(1-\alpha)}{\rho_L}\frac{\partial \rho_L}{\partial h_L}C_5$$
$$C_2 = -(f_{w,L} + f_{w,G}) - \rho_m g\frac{dZ}{dx}$$
$$C_3 = \frac{\rho_m}{\rho_L \rho_G}\Gamma_{i,G} - \alpha(1-\alpha)\left[\frac{1}{\rho_G}\frac{\partial \rho_G}{\partial h_G}C_4 - \frac{1}{\rho_L}\frac{\partial \rho_L}{\partial h_L}C_5\right]$$
$$C_4 = \frac{q_{i,G} + q_{w,G} + f_{w,G}u}{\alpha \rho_G}$$
$$C_5 = \frac{q_{i,L} + q_{w,L} + f_{w,L}u}{(1-\alpha)\rho_L} \tag{29}$$

The corresponding characteristic and compatibility relations are

$$C^+: dx = (u+a)\,dt; \quad dP + \rho a\,du = (\rho a^2 C_1 + aC_2)\,dt$$
$$C^-: dx = (u-a)\,dt; \quad dP - \rho a\,du = (\rho a^2 C_1 - aC_2)\,dt$$
$$PP: dx = u\,dt; \quad d\alpha - \alpha(1-\alpha)\left[\frac{1}{\rho_L a_L^2} - \frac{1}{\rho_G a_G^2}\right]dP = C_3\,dt$$
$$PP: dx = u\,dt; \quad dh_G - \frac{1}{\rho_G}dP = C_4\,dt$$
$$PP: dx = u\,dt; \quad dh_L - \frac{1}{\rho_L}dP = C_5\,dt \tag{30}$$

3.3. Characteristic form of the Isentropic flow equations in the air phase

The assumption for the existence of isentropic conditions is (19):

$$\frac{Ds_{air}}{Dt} = 0 \tag{31}$$

In general, two thermodynamic properties are required to define a thermodynamic state, e.g., select $\rho = \rho(P,s)$, thus

$$\frac{D\rho}{Dt} = \left(\frac{\partial \rho}{\partial P}\right)_s \frac{DP}{Dt} + \left(\frac{\partial \rho}{\partial s}\right)_P \frac{Ds}{Dt} \tag{32}$$

Combining Eqs. (31), (32) and (25) yields

$$\frac{D\rho}{Dt} = \frac{1}{a^2}\frac{DP}{Dt} \tag{33}$$

Therefore, the two thermodynamic properties that would appear in the characteristic equations are the pressure and the density. The equations of motion are written for isentropic conditions in characteristic form as:

$$\frac{D^+P_{air}}{Dt} + \rho_{air}a_{air}\frac{D^+u_{air}}{Dt} = \rho a_{air}^2 C_6 + a_{air}C_7$$
$$\frac{D^-P_{air}}{Dt} + \rho_{air}a_{air}\frac{D^-u_{air}}{Dt} = \rho a_{air}^2 C_6 - a_{air}C_7$$
$$\frac{D\rho_{air}}{Dt} - \frac{1}{a_{air}^2}\frac{DP_{air}}{Dt} = 0 \tag{34}$$

The C_i are given by

$$C_6 = -u_{air}\frac{1}{A}\frac{dA}{dx}$$
$$C_7 = -f_{w,L}$$

The characteristic and compatibility relations are

$$C^+: dx = (u_{air} + a_{air})\,dt;$$
$$dP_{air} + \rho_{air}a_{air}\,du_{air} = (\rho_{air}a_{air}^2 C_6 + a_{air}C_7)\,dt$$
$$C^-: dx = (u_{air} - a_{air})\,dt; \tag{35}$$
$$dP_{air} - \rho_{air}a_{air}\,du_{air} = (\rho_{air}a_{air}^2 C_6 - a_{air}C_7)\,dt$$
$$PP: dx = u_{air}\,dt;\ dP_{air} - a_{air}^2\,d\rho_{air} = 0$$

There are three characteristics (waves C^+, C^- and the particle path PP) with three corresponding equations. Excluding very special cases, this set of equations can only be solved numerically.

3.3.1. The shock formation

The formation of the shock is examined on the base of the characteristic analysis. At a non-uniform flow field the advanced information waves C^+ exhibit characteristics that either converge or diverge. The formation of a shock wave is attributed to the intersection of two characteristic lines [28].

3.4. The solution procedure

A numerical-solution method based on the method of characteristics was employed for the investigation of the BLEVE problem. The method is used for the solution of the governing equations for unsteady one-dimensional of two-phase flow as well as for the airflow, derived at the previous sections. The method of characteristics was also employed to study and define the location of the shock wave and to calculate the fluid particle path and properties passing the shock wave. For this purpose, a special numerical scheme was derived [23].

The procedure is employed for the numerical integration of the characteristic and compatibility equations, using an explicit numerical scheme. Expanding grid spacing is utilized for the BLEVE problem, based on particle-path tracing algorithm where constant time intervals, Δt, are used [33].

4. The comparison procedure of the model against TNT models

The BLEVE's shock wave pressure and the blast effect are usually presented in terms of energy in the form of TNT equivalents [4,20]. The energy calculations are based on the assumption that adiabatic expansions of the content take place, as the pressure decreases from the initial pressure toward the ambient atmospheric pressure. Details of the energy and the TNT equivalence models are presented in Appendix A.

These models are essentially empirical, and are actually the only practical model available. To express the released energy, W_{flash}, in terms of equivalent kilograms of TNT (where the specific explosion TNT energy was taken as 4650 kJ/kg [4]) the following conversion relationship was used: m_{TNT} [kg-TNT] $= 24.1 \times 10^{-3} \times m_{\text{flash}}$ [kJ].

The principal parameter of a blast wave from an explosion is the side-on overpressure, ΔP_{shock}, in the far field. Therefore this parameter constitutes the basis for the equivalent TNT explosion. The values of the side-on overpressure for TNT explosions in free air are correlated as a function of the scaled distance, z_{SD} (Appendix A).

The cubic root index in the scaling law originates from the energy radial expansion with a volumetric expansion that is proportional to third power of the radius. To analyze the results of the current one-dimensional plane expansion model, the pertinent scaling law is defined as

$$z_{\text{SD}} = \frac{r}{m_{\text{TNT}}} \tag{36}$$

where r is the distance [m], m_{TNT} is the mass of explosive (TNT) [kg-TNT] and z_{SD} is the modified scaled distance [m/kg-TNT].

The blast correlation is given in Fig. 7, and is referred to as TNT curve [2]. The numerical results of the model were analyzed using blast wave scaling and TNT curves to find the equivalent mass of TNT of a particular BLEVE scenario.

The numerically calculated shock wave overpressure at a certain distance was used for locating the corresponding scaled distance from the TNT curve. Setting the scaled distance in Eq. (36), for the Cartesian one-dimensional problem, the equivalent mass of TNT was found. The latter was then compared to the equivalent mass of TNT that was obtained from the energy models [4,20]. Obviously, in all these one-dimensional analyses, parameters such as mass and energy are calculated per unit area.

5. Results

The current model was employed to study the conditions that could lead to a boiling liquid expanding vapor explosion (BLEVE) and its possible consequences. The model was utilized to predict the behavior of the shock wave formed by the liquid–vapor two-phase mixture 1D plane expansion in air.

The results of the numerical calculations for the expansion with water as a working material are presented. Finally, the current model predictions are compared to those of simple energy models. The comparison is based on TNT equivalence model.

5.1. Model validation

The predictions of the BLEVE numerical model were first analyzed for the two well-known cases. The two-phase model was tested against experimental results of blowdown case, i.e. flashing flow through a channel. The blowdown problem was studied through a finite channel for various initial and boundary conditions, and was tested successfully against two sets of experimental data [31].

Likewise, the BLEVE model results were analyzed for the particular case of an expanding gas (a shock-tube problem) [33]. The results were successfully compared against two exact analytical solutions for two standard test problems. For such events, the model calculates and determines both the shock wave position and the pressure differential across it.

5.2. BLEVE problem

After code validation with an expanding gas, the BLEVE model was used to analyze the rapid depressurization characteristics of a liquefied gas.

5.2.1. BLEVE: Semi-infinite regions

The case studied is of two semi-infinite regions of compressed water in contact with air. The model was applied to study effects of different initial temperatures on the flow response including the formation of shock waves. The initial thermodynamic conditions were those of saturated water.

Profiles of the flow properties evaluation during BLEVE for two cases are presented for three different times. The first results are for a relatively low initial temperature, $T_0/T_c = 0.70$, and $n_{B,0} = 3 \times 10^7$ m^{-3} (Fig. 3). Then, results are presented for a high initial temperature, $T_0/T_c = 0.95$, and $n_{B,0} = 10^{12}$ m^{-3} (Fig. 4). In these figures, the pressure, velocity, velocity of sound and Mach number, are plotted as a function of the position x, where $x = 0$ is the initial location of the initial the water/air boundary.

Behind the rarefaction wave the mixture pressure increases owing to vapor generation. For relatively low initial temperature (Fig. 3), the pressure buildup increases above the rarefaction wave pressure, but not enough to form a shock wave. For high initial temperatures (Fig. 4), the pressure buildup is substantial, but does not exceed the rarefaction wave pressure (the latter coincides with the spinoidal). That buildup however is powerful enough to form a shock wave. Notice that the expansion from low-pressure conditions produces a local minimum with a subsequent net pressure buildup, owing to rapid bubble growth. However, that growth is comparatively weak to produce a net pressure buildup when the expansion is from high-pressure conditions. Nonetheless, it noticeably slows down the depressurization rate.

If the failure occurs under the condition of a relatively low initial temperature (Fig. 3), the depressurization is characterized by rapid boiling. The contact surface velocity between vapor and air is well below values that are required for shock wave formation. In contrast, failures occurring at high initial temperatures cause rapid depressurizations that could lead to explosions and shock wave formation (Fig. 4). At high initial temperatures the ‘‘expan-

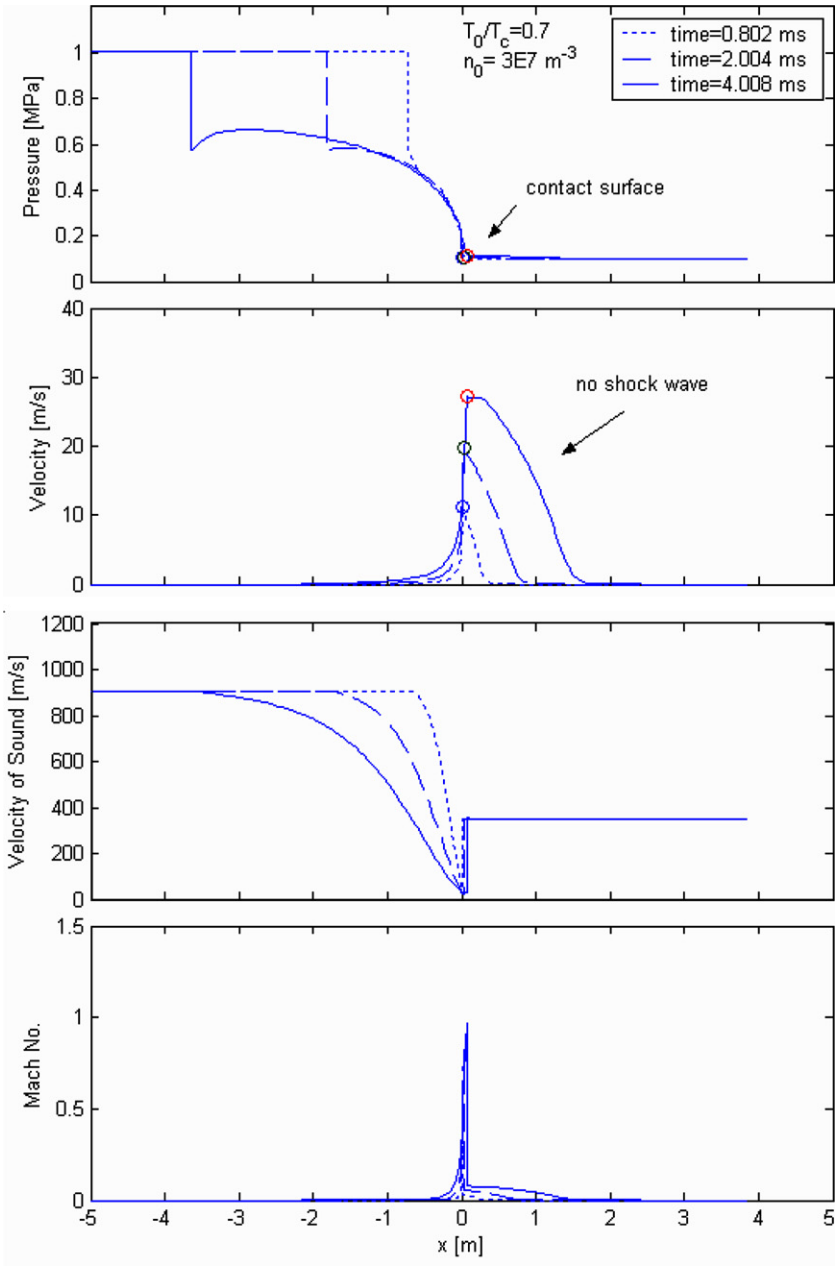

Fig. 3. Flow properties evaluation for $T_0/T_c = 0.70$ and $n_{B,0} = 3 \times 10^7$ m^{-3}.

sion fan" region contains a moving sonic point $u = a$ at $x = 0$ (Fig. 4). Beyond this region, both, the two-phase mixture and the air (near the contact surface) are supersonic.

Applying the model to test the effects of various initial temperatures revealed that shock wave formation occurs at temperatures higher than $T_0/T_c \sim 0.90$. Shock strength time histories are presented in Fig. 5 for various initial temperatures.

It was found that, shortly after formation, the shock strength increases rapidly with time, and thereafter increases gradually. The shock wave strengthens with time owing to continuous vapor generation. This is in contrast to the characteristics of the expanding air where the shock wave strength reaches a constant value after a short acceleration stage. Notice that higher initial temperatures produce stronger shock waves.

The formation of the shock at $T_0/T_c = 0.90$ occurs after ~ 1.5 ms. At higher initial temperatures, the shock formation begins slightly sooner, nonetheless its inception begins essentially after a period of approximately 0.5 ms. (necessary for the material particles acceleration).

5.2.2. BLEVE formation

The results of the present numerical model seemed to be consistent with Reid's hypothesis. The formation of the BLEVE was found to occur at the initial temperature predicted by Reid. This is impressive of great consequence

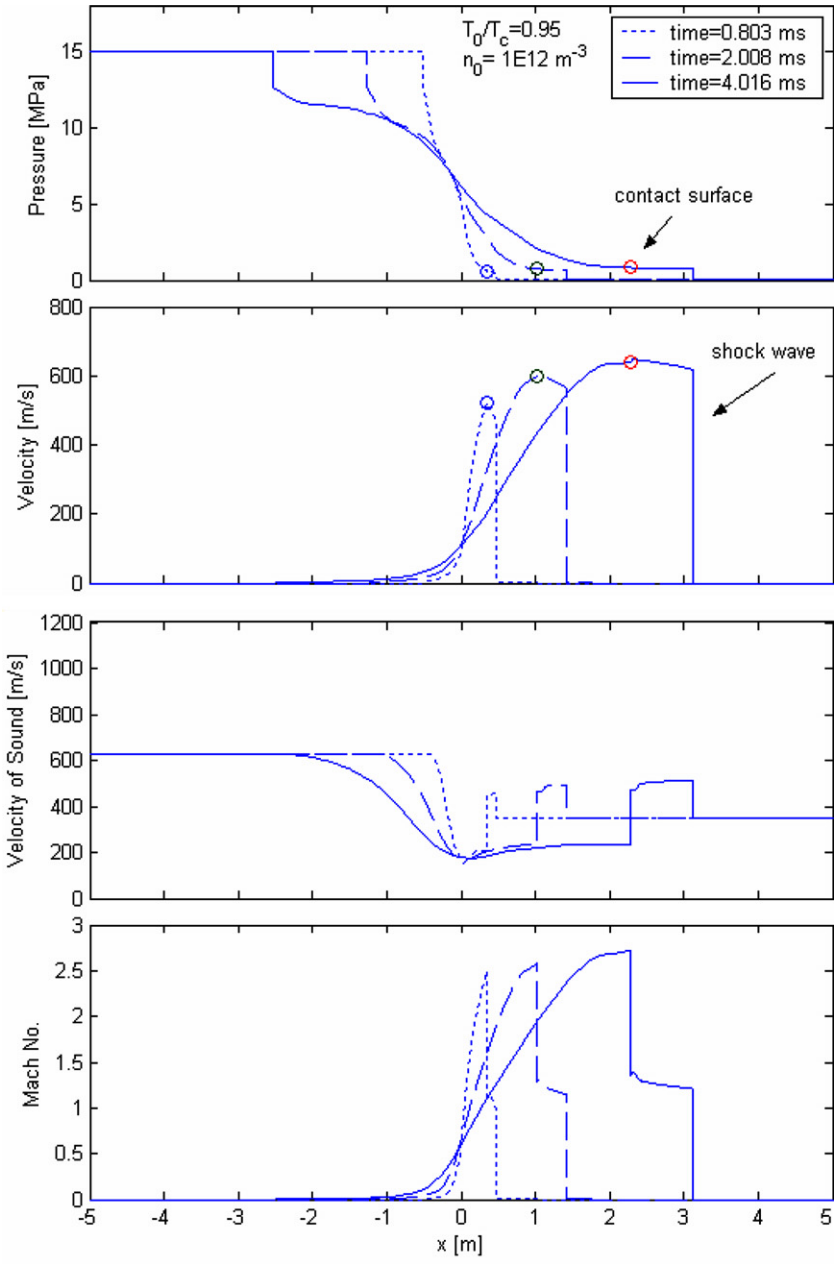

Fig. 4. Flow properties evaluation for $T_0/T_c = 0.95$ and $n_{B,0} = 10^{12}$ m^{-3}.

since the present results are based on the numerical solution of the process dynamics and not merely on thermodynamic ad-hoc considerations. The model results show that the BLEVE is formed at these high temperatures by the combined influence of high nucleation site number density and high vapor pressure.

In contrast with gas shock wave tube problem, an analytical solution for the BLEVE problem is highly complex since the characteristic lines are no longer of constant values (such as in ideal gas case). The two-phase characteristic equations are changing with time along the characteristic lines. The analysis of the "expansion fan" region for a two-phase boiling mixture requires integration of the equations along these lines. This was accomplished numerically by the current model.

5.3. Comparison the numerical results with the energy models

In this section, the model addresses the case of a finite liquid region, such as a liquid body in a vessel. Predictions of the model are compared against results of a simple energy models. The comparison is based on TNT equivalence model.

The calculation of the TNT equivalence of the numerical results is based on calculating the shock wave overpressure at a certain distance from the explosion site. This was done for a given vessel length of compressed liquid at a specified temperature.

The BLEVE model was applied to study effects of the initial temperature on the blast wave characteristics at the far field. For a liquid length of 0.05 m, the model was

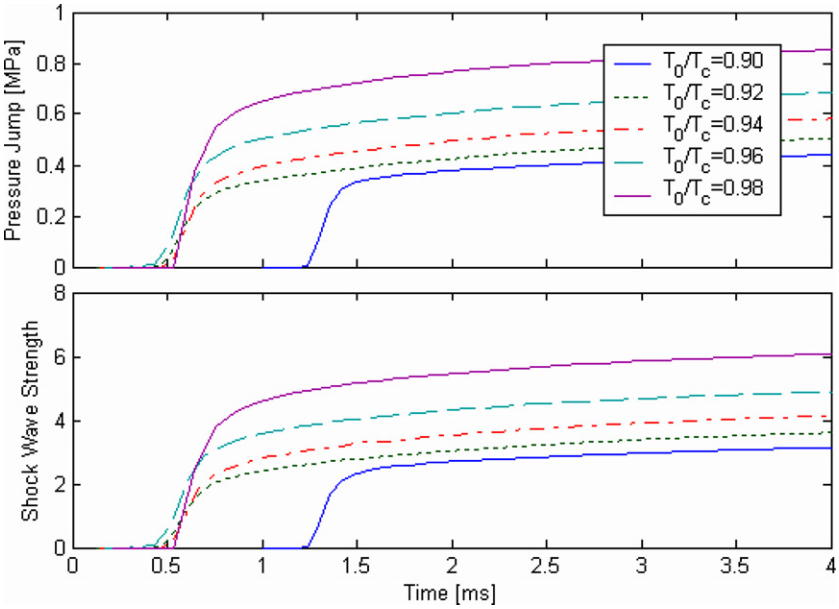

Fig. 5. Shock wave strength history during BLEVE for various initial temperatures.

applied for two initial temperatures, $T_0/T_c = 0.90$ and $T_0/T_c = 0.95$. The calculated shock intensity as a function of distance is presented in Fig. 6, for the two initial temperatures. The shock properties that are presented are the shock over-pressure and the dimensionless shock strength, Π. The shock wave has a profile in which the pressure rises sharply to a peak value and then gradually tails off. The shock strength parameters decay with distance.

For the distance of 20 m, a comparison of results between those of the present model and the energy model was made. The comparison is based on calculation of the TNT equivalence for both models. The comparison is summarized in Table 1 for the two initial temperatures.

Relatively large differences were found between the numerical model and the reversible energy model predictions. However the comparison against the irreversible energy model revealed a much closer match. For $T_0/T_c = 0.90$, the numerical prediction was 0.38 [kg-TNT/m^2] the reversible energy model [4] prediction was 1.68 [kg-TNT/m^2] and the irreversible energy model [20] prediction was 0.66 [kg-TNT/m^2]. For $T_0/T_c = 0.95$, the numerical prediction was 0.44 [kg-TNT/m^2], the reversible energy model [4] prediction was 1.43 [kg-TNT/m^2] and the irreversible energy model [20] prediction was 0.69 [kg-TNT/m^2].

The simple energy models tend to over-estimate the BLEVE consequences as compared to the numerical model

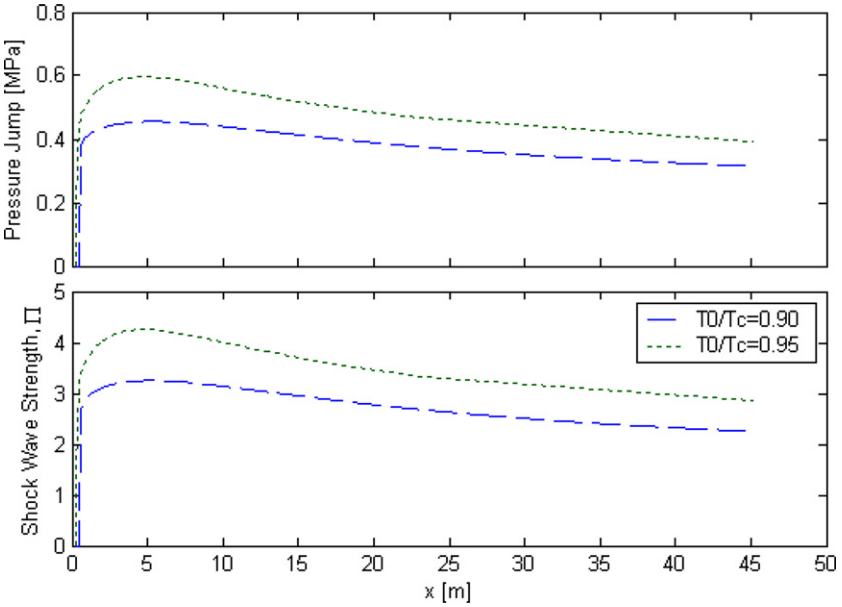

Fig. 6. Shock wave dissipation with distance during BLEVE for two initial temperatures.

Table 1
TNT equivalence at distance of 20 m for initial liquid length $L_0 = 0.05$ m

Initial temperature	T_0/T_c	–	0.90	0.95
Numerical results				
Shock strength	Π	–	2.75	3.44
Pressure jump	ΔP_{shock}	[MPa]	0.39	0.48
Scaled distance	Z_{SD}	[m/kg]	45	52
TNT equivalence	m_{TNT}	[kg-TNT/m^2]	0.38	0.44
Energy model – reversible (Prugh's model [4])				
Expansion energy	W_{flash}	[kJ/m^2]	7845	6677
TNT equivalence	m_{TNT}	[kg-TNT/m^2]	1.68	1.43
Energy model – irreversible (Planas-Cuchi's model [20])				
Expansion energy	W_{flash}	[kJ/m^2]	3080	3238
TNT equivalence	m_{TNT}	[kg-TNT/m^2]	0.66	0.69

results. The major reason for this discrepancy lies in the difference of the vapor formation mechanisms that the models are based on. According to the energy model, the liquid flashes instantaneously and the entire vapor is formed prior to the expansion. Furthermore, the vapor is assumed to be at the initial vapor pressure. However, in the actual case, there is a continuous process of vapor formation during expansion. Therefore the initial pressure of the newly generated vapor is smaller than the vessel initial pressure.

Note that the characteristics of the blast from the explosion of TNT charge are significantly different from those of other explosions. To substantiate that, consider that the pressure developed by a TNT explosion, while still in confinement within its initial boundaries, is on the order of half a million bar. This is well in excess of what could be experienced in a BLEVE. The latter energy develops more gradually and is spread over a much larger scale.

Comparing the profile of the peak overpressure from a TNT explosion with that from a BLEVE explosion, both, in the near field and in the far fields, the peak overpressure of the TNT explosion is higher. One consequence of this is that the use of the energy model is over-predicting the risks.

6. Conclusions

In the current study, a 1D plane numerical model was developed for estimating the thermodynamic and the dynamic state of the boiling liquid during a BLEVE event. Based on the choice of the initial nucleation sites density, the model predicts, simultaneously, the bubble growth processes in the liquid at the superheat-limit state, the front velocity of the expanding liquid, and the shock wave pressure formed by the liquid expansion through the air. A novel model is given which describe the coupling of two-phase flashing flow with compressible airflow.

The simple energy model tends to over-estimate the BLEVE scenario consequences as compared to numerical model predictions. Relatively large differences were also found between the numerical model and the reversible energy model predictions. However, the irreversible energy model predictions matched much closer the numerical model results.

The study reveals what are the important mechanisms that dominate two-phase blowdown and BLEVE accidents. The model reveals the characteristics of a BLEVE scenario in a tunnel, or within any other type of cylindrical conduit. The developed models enable calculations of the required input data necessary for running contaminants dispersion codes. They are therefore important computational tools for environmental safety assessments.

Appendix A. Energy models

TNT equivalent models are frequently used to scale various types of explosions. The modeling is based on estimating the energy of the explosion, calculating the TNT equivalent and then treating the explosion as if it was one from a TNT charge.

In the current appendix a simple energy models for a BLEVE scenario and blast wave parameters are presented. The energy of expansion and the blast wave parameters were used in terms of TNT equivalents. This approach was used as a first order evaluation and validation of the numerical results.

A.1. BLEVE energy model: Reversible

During a BLEVE explosion, the mechanical energy contained inside a bursted vessel is suddenly released. The substance contained in the vessel instantaneously increases in volume due to expansion of the vapor already existing in the vessel at the moment of the explosion and to the partial vaporization – practically instantaneous (flash) – which the superheated liquid undergoes. This expansion will give rise to a pressure wave (blast).

An expression for calculating the energy released during an adiabatic and reversible (isentropic) expansion ($PV^{\gamma} = \text{constant}$) of gas from a volume V_0 and pressure P_0 to atmospheric pressure P_{atm} is [4]:

$$W_{flash} = \int P\,dV = \frac{P_0 V_0}{\gamma - 1}\left[1 - \left(\frac{P_{atm}}{P_0}\right)^{\frac{\gamma-1}{\gamma}}\right] \tag{37}$$

where γ is the specific heat ratio $\gamma = C_P/C_V$. (for water vapor $\gamma = 1.32$).

To estimate the energy released from the rupture of a liquefied gas container, the weight of liquid that flashes to vapor during depressurization to atmospheric pressure is estimated. The volume of the released vapor, at the initial container pressure, is comprised of the flash vapor and the vapor contained within the initial container free space, which is

$$V_0 = V_G + V_L\left(\chi_{flash}\frac{\rho_L}{\rho_G}\right) \tag{38}$$

where χ_{flash} is the flashing fraction (the mass fraction of the liquid that vaporized), V_L and V_G are the initial liquid volume and the initial vapor volume, respectively.

A.1.1. Flashing fraction

The sudden pressure drop around a subcooled liquid triggers a flashing process followed by an adiabatic expansion of the released vapor cloud. The flashing fraction is obtained from the following energy balance

$$h_{LG}\,dm_G = C_{P,L}\,dT \tag{39}$$

The dependence of the latent-heat and specific-heat on temperature are,

$$\frac{h_{LG}}{(h_{LG})_0} = \left(\frac{T_c - T}{T_c - T_0}\right)^{0.38}, \quad \frac{C_{P,L}}{(C_{P,L})_0} = \left(\frac{T_c - T}{T_c - T_0}\right)^{-0.24} \tag{40}$$

where T_0 is a reference temperature and T_c is the critical temperature [4]. The expression for the latent-heat is known as Watson relation.

From the integration of the energy balance (39), from T_0 to the boiling temperature at atmospheric pressure T_b, an expression for the flashing fraction is obtained

$$\chi_{flash} = 1 - \exp\left\{-2.63\left(\frac{C_{P,L}}{h_{LG}}\right)(T_c - T_b)\left[1 - \left(\frac{T_c - T_0}{T_c - T_b}\right)^{0.38}\right]\right\} \tag{41}$$

In this equation the term $(C_P, Lh_{LG})(T_c - T_b)$ is the vaporization factor (equals 0.51 for water).

A.2. BLEVE energy model: Irreversible

Planas-Cuchi et al. [20] proposed a new approach, which is based on – more realistic – assumption of an adiabatic and irreversible expansion process. The irreversible expansion work is $-P_\infty \Delta V$, where P_∞ is the pressure just after the expansion (usually P_{atm}) and ΔV being the variation in volume of the whole content of the vessel when it changes from the explosion state to the hypothetical final state. On the other hand, for adiabatic process, this work must be equal to the variation in internal energy of the vessel content ΔE:

$$W_{flash} = -P_\infty \Delta V = \Delta E \tag{42}$$

Taking into account the mass and energy balances, the above equation is

$$-\Delta E = (e_L - e_G)m_T\chi - m_T e_L + E_0 \tag{43}$$

$$P_\infty \Delta V = P_\infty[(v_L - v_G)m_T\chi - m_T v_L + V_0] \tag{44}$$

where e_L, e_G are the internal energy at the final state of the liquid and the vapor respectively, v_L, v_G are the specific volume at the final state of the liquid and the vapor respectively, χ is the quality at the final state, m_T is the overall mass in the vessel, V_0 and E_0 are the initial volume and internal energy respectively. From these two equations,

$$x = \frac{m_T P_\infty v_L - V_0 P_\infty + m_T u_L - E_0}{[(u_L - u_G) - (v_G - v_L)P_\infty]m_T} \tag{45}$$

By substitution the value of x in (43) or (44) the W_{flash} is found.

A.3. Blast wave

One of the main effects of an explosion is the creation of a shock wave, or a blast wave. This blast wave is in effect a traveling hazardous overpressure wave that could injure people and damage equipment and buildings.

In the current section the blast wave scaling law and the blast overpressure correlation are presented. These parameters are used to analyze the numerical results, in terms of TNT equivalents.

A.3.1. Energy of explosion of TNT

The values used for the explosion energy of TNT lie in the range 4140–4650 kJ/kg-TNT [2]. The specific explosion TNT energy is commonly taken as 4650 kJ/kg [4].

A.3.2. TNT curve

The blast characteristics of a TNT explosion are often used in the modeling of other types of explosion. There is much more available information on explosions of explosives, particularly TNT, than on explosions of other materials (for instance, such as for vapor explosions).

The principal one parameter of the blast wave from TNT explosion is the side-on overpressure, ΔP_{shock}, in the far field. The values of this parameter are presented as a function of the scaled distance, for a free air burst (spherical symmetry). The blast correlation is given in Fig. 7, called TNT curve [2]. The curve utilizes a damage classification based on the damage to dwelling houses in the Second World War.

A.3.3. Blast scaling

The characteristics of the blast wave produced by an explosion are generally determined by the application of the scaling laws [2]. For the blast wave caused by explosion, the scaling relationship most widely used is the 'cube root' law. This law states that when two charges of the same explosive material and geometry but of different size are detonated in the same atmosphere, self-similar shock waves are produced at the same-scaled distances. The scaled distance is defined as

$$z_{SD} = \frac{r}{m_{TNT}^{1/3}} \tag{46}$$

where r is the spatial distance, m_{TNT} is the mass of explosive and z_{SD} is the scaled distance. It should be noted that the scaled distance is not dimensionless.

Strictly the relevant scaling variable is the energy W_{flash}, rather than the mass of explosive m_{TNT}. But for particular explosive it is commonly assumed that the energy released is proportional to the explosives mass.

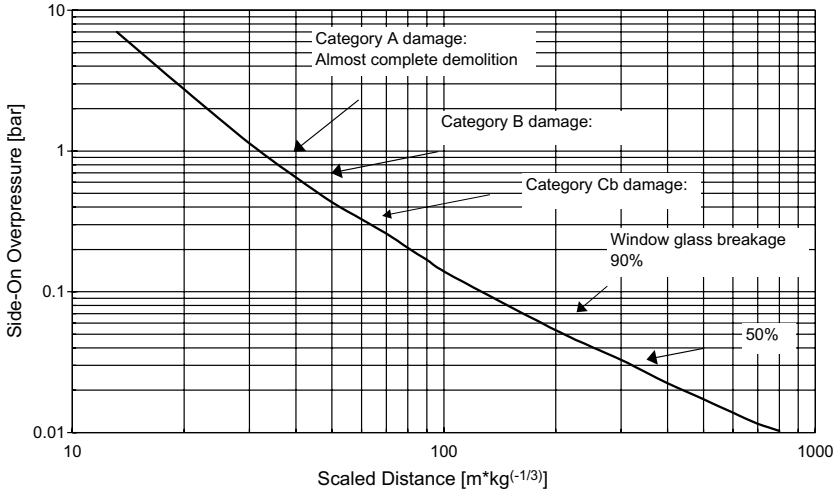

Fig. 7. Peak side-on overpressure for TNT-TNT curve [2].

The cube root index in the scaling law is related to the fact that the energy is deposited into a spherical, or hemispherical, region, the volume of which varies with the cube of the radius. To analyze the results for the one-dimensional plane expansion problem, the pertinent scaling law, for evaluating the numerical model, was defined as

$$z_{\mathrm{SD}} = \frac{r}{m_{\mathrm{TNT}}} \tag{47}$$

Obviously in those analyses, parameters such as mass and energy are calculated per unit area.

References

[1] I.R.M. Leslie, A.M. Brik, State of the art review of pressure liquefied gas container failure modes and associated projectile hazards, J. Hazard Mater. 28 (1991) 329–365.
[2] F.P. Lees, Loss Prevention in the Process Industries, Vol. 1–3, Butterworth-Heinemann, Oxford, 1996.
[3] T.A. Klets, Protect Pressure Vessels from Fire, Hydrocarb. Proc. 56 (1977) 98.
[4] R.W. Prugh, Quantity BLEVE Hazards, Chem. Eng. Prog. 87 (2) (1991) 66–71.
[5] C.A. McDevitt, C.K. Chen, F.R. Steward, K.N. Tenneankore, Initiation step of boiling liquid expanding vapor explosions, J. Hazard. Mater. 25 (1990) 169–180.
[6] G.A. Melhem, P.A. Croce, H. Abraham, Data summary of the National Fire Protection Association's BLEVE tests, Process Safety Progr. 12 (2) (1993) 76–82.
[7] J.E.S. Venart, G.A. Rutledge, K. Sumathiphala, K. Sollows, To BLEVE or not to BLEVE: Anatomy of boiling liquid expanding vapor explosion, Process Safety Progr. 12 (2) (1993) 67–70.
[8] J. Stawczyk, Experimental evaluation of LPG tank explosion hazards, J. Hazard. Mater. B 96 (2003) 189–200.
[9] C.R. Reid, Possible mechanism for boiling liquid expanding vapor explosion or BLEVE, Science 203 (1979) 1263–1265.
[10] V.P. Skripov, Metastable Liquids, Wiley, New York, 1974, English translation.
[11] R.P. Anderson, D.R. Armstrong, Comparison between vapor explosion models and recent experimental results, AIChE Symp. Series 70 (138) (1974) 31–47.
[12] W.E. Martinsen, D.W. Johnson, W.F. Terrel, BLEVE's: their causes effects and prevention, Hydrocarbon Proces. 5 (11) (1986) 141–148.
[13] C.A. McDevitt, F.R. Steward, J.E.S. Venart, What is a BLEVE? in: The 4th Technical Seminar on Chemical Spills Proceedings, Canadian Transport Commission, Toronto, Ottawa, Ont., 1987, pp. 137–147.
[14] J.A. Davenport, Hazards and protection of pressure storage and transportation of LP-gas, J. Hazard. Mater. 20 (1988) 3–19.
[15] V. Dunn, BLEVE: the propane cylinder, Fire Eng. 131 (1988) 63–70.
[16] C.M. Yu, J.E.S. Venart, The boiling liquid collapsed bubble explosion (BLCBE): a preliminary model, J. Hazard. Mater. 46 (1996) 197–213.
[17] A.C. Van den Berg, M.M. Van den Voort, J. Weerheijm, N.H.A. Versloot, Expansion-controlled evaporation: a safe approach to BLEVE blast, J. Loss Prev. Process Ind. 17 (2004) 397–405.
[18] A.C. Van den Berg, M.M. Van den Voort, J. Weerheijm, N.H.A. Versloot, BLEVE blast by expansion-controlled evaporation, J. Loss Prev. Process Ind. 25 (2006) 44–51.
[19] P. Deligiannis, J.W. Cleaver, Blowdown from a vented partially full vessel, Int. J. Multiphase Flow 22 (1) (1996) 55–68.
[20] E. Planas-Cuchi, J.M. Salla, J. Casal, Calculating overpressure from BLEVE explosions, J. Loss Prevent. Ind. 17 (2004) 431–436.
[21] G.A. Pinhasi, A. Dayan, A. Ullmann, Modeling of flashing two-phase flow, Rev. Chem. Engng. 21 (3–4) (2005) 133–264.
[22] V.N. Blinkov, O.C. Jones Jr., B.I. Nigmatulin, Nucleation and flashing in nozzles – 2: Comparison with experiments using a five-equation model for vapor void development, Int. J. Multiphase Flow 19 (1993) 943–986.
[23] G.A. Pinhasi, Source Term Modeling of Gas and Liquid Releases from a Breached Pressure Vessel, Ph.D. Thesis, Tel-Aviv University, 2001.
[24] D.A. Labuntzov, B.A. Lolchugin, V.S. Golovin, E.A. Zakharova, L.N. Vladimirova, High speed camera investigation of bubble growth for saturated water boiling in a wide range of pressure variations, Thermophys. High Temp. 2 (1964) 446–453.
[25] O.C. Jones Jr., N. Zuber, Bubble growth in variable pressure fields, J. Heat Transfer, ASME 100 (1978) 453.
[26] B.J.C. Wu, N. Abuaf, P. Saha, A study of nonequilibrium flashing of water in a converging–diverging nozzles, Vol. 2 – Modeling. Reports NUREG/CR-1864 and BNL-NUREG-51317, 1981.
[27] C.W. Solbring, J.H. McFadden, R.W. Lyczkowski, E.D. Hughes, Heat transfer and friction correlations required to describe steam–water behavior in nuclear safety studies, AIChE Symp. Ser. 74 (174) (1978) 100–128.
[28] P.A. Thompson, Compressible-Fluid Dynamics, McGraw-Hill, New York, 1972.
[29] C.B. Laney, Computational Gasdynamics, Cambridge, 1998.
[30] E. Elias, P.L. Chambre, Flashing inception in water during rapid decompression, J. Heat Transfer 115 (1993) 231–238.

[31] G.A. Pinhasi, A. Dayan, A. Ullmann, Numerical model for bubbles break-up during blowdown, in: 43rd Aerospace Sciences Meeting and Exhibit, 10–13 January, Reno Nevada, AIAA 2005-0383, 2005.
[32] R.L. Ferch, Method of characteristics solution for non-equilibrium transient flow-boiling, Int. J. Multiphase Flow 5 (1979) 265–279.
[33] G.A. Pinhasi, A. Dayan, A. Ullmann, A numerical model for boiling liquid expanding vapor explosion (BLEVE), in: 42nd Aerospace Sciences Meeting and Exhibit, 6–9 January, Reno Nevada. AIAA 2004-161, 2004.